REPORT DOCUMENTATION PAGE

Form Approved
OMB No. 0704-0188

1. REPORT DATE (DD-MM-YYYY)	2. REPORT TYPE	3. DATES COVERED (From - To)
June 2003	Conference Proceedings	5/02 - 6/03

4. TITLE AND SUBTITLE
Dynamics of HF(v,J) Chemiluminescence and Lasing by Infrared Hyperspectral Imaging

5a. CONTRACT NUMBER
F29601-02-C-0111

5b. GRANT NUMBER

5c. PROGRAM ELEMENT NUMBER
65502F

6. AUTHOR(S)
S. J. Davis, W. T. Rawlins, D. B. Oakes, G. Dadusc, and D. X. Hammer

5d. PROJECT NUMBER
6001

5e. TASK NUMBER
MD

5f. WORK UNIT NUMBER
AG

7. PERFORMING ORGANIZATION NAME(S) AND ADDRESS(ES)

Physical Sciences, Inc.
20 New England Business Center
Andover, MA 01810

8. PERFORMING ORGANIZATION REPORT NUMBER

9. SPONSORING / MONITORING AGENCY NAME(S) AND ADDRESS(ES)

Air Force Research Laboratory
Directed Energy Directorate
3550 Aberdeen Ave. SE
Kirtland AFB, NM 87117

12. DISTRIBUTION / AVAILABILITY STATEMENT
Approved for public release; distribution is unlimited

13. SUPPLEMENTARY NOTES
Proceedings of the 34th AIAA Plasmadynamics and Lasers Conference
AIAA-2003-3756

14. ABSTRACT

This paper presents results from a continuing investigation of mixing flowfields and optical gain profiles in HF chemical laser systems by infrared hyperspectral imaging. Chemiluminescent F + H2 reacting flowfields and chemical laser output beams are imaged at a series of wavelengths, 2.6 to 2.9 microns, by a low-order, spectrally scanning Fabry-Perot interferometer mated to an infrared camera. The resulting hyperspectral data cubes define the spectral and spatial distributions of the emission. High-resolution images can be processed to determine spatial distributions of the excited state concentrations of the product HF(v,J), as well as spatial distributions of gain on specific laser transitions. This paper describes the instrumentation and its application to detailed observations of reactant mixing and energy transfer in the product HF(v,J), using a low-pressure laboratory reactor developed at Physical Sciences, Inc. (PSI). The measurements confirm that the PSI reactor generates inverted populations of HF(v,J).

15. SUBJECT TERMS
HF chemical lasers, chemical laser diagnostics, hyperspectral imaging, reactive flows

16. SECURITY CLASSIFICATION OF:			17. LIMITATION OF ABSTRACT	18. NUMBER OF PAGES	19a. NAME OF RESPONSIBLE PERSON
a. REPORT	b. ABSTRACT	c. THIS PAGE			Gerald C. Manke II
Unclassified	Unclassified	Unclassified	Unlimited	10	19b. TELEPHONE NUMBER (include area code) 505-853-2674

AIAA 2003-3756

Dynamics of HF(v,J) Chemiluminescence and Lasing by Infrared Hyperspectral Imaging

S.J. Davis, W.T. Rawlins, D.B. Oakes, G. Dadusc,
and D.X. Hammer
Physical Sciences Inc.
20 New England Business Center
Andover, MA 01810

34th AIAA Plasmadynamics and Lasers Conference
23-26 June 2003
Orlando, FL

DYNAMICS OF HF(v,J) CHEMILUMINESCENCE AND LASING BY INFRARED HYPERSPECTRAL IMAGING

S.J. Davis*, W.T. Rawlins†, D.B. Oakes‡, G. Dadusc§, and D.X. Hammer§
Physical Sciences Inc.
Andover, MA 01810

Abstract

This paper presents results from a continuing investigation of mixing flowfields and optical gain profiles in HF chemical laser systems by infrared hyperspectral imaging. Chemiluminescent $F + H_2$ reacting flowfields and chemical laser output beams are imaged at a series of wavelengths, 2.6 to 2.9 μm, by a low-order, spectrally scanning Fabry-Perot interferometer mated to an infrared camera. The resulting hyperspectral data cubes define the spectral and spatial distributions of the emission. High-resolution images can be processed to determine spatial distributions of the excited state concentrations of the product HF(v,J), as well as spatial distributions of gain on specific laser transitions. This paper describes the instrumentation and its application to detailed observations of reactant mixing and energy transfer in the product HF(v,J), using a low-pressure laboratory reactor developed at Physical Sciences Inc. (PSI). The measurements confirm that the PSI reactor generates inverted populations of HF(v,J).

Introduction

Chemical lasers rely on exoergic chemical or energy transfer reactions to produce population inversions in the product species. To function efficiently, these systems must have rapid and effective mixing of the reagent gas streams. The coupled kinetics and mixing dynamics are often difficult to diagnose, especially for infrared systems such as HF. The HF laser uses the exoergic reaction

$$F + H_2 \rightarrow H + HF(v,J) \qquad (1)$$

to generate partial inversions between several rovibrational levels in different vibrational states. This results in lasing on several lines of the HF(Δv=1) fundamental band in the 2.5 to 3 μm spectral region. In efficient HF lasers, most intense lasing takes place on the v=2 to v=1 and v=1 to v=0 bands, for several rotational transitions. The allowed fundamental-band radiative transitions which occur for HF are from upper states (v',J') to lower states (v'-1, J'-1) ("R-branch") and (v'-1, J'+1) ("P-branch"). Partial inversion of the vibrational and rotational state populations leads to laser oscillation on P-branch rotational lines, i.e., (v', J') → (v'-1, J'+1). These transitions are denoted as $P_{v'}(J'+1)$. A typical HF laser spectrum[1] is shown in Figure 1, and the transitions are labeled. For high-power HF lasers, the relevant lines of interest are the $P_1(6) - P_1(9)$ and $P_2(5) - P_2(9)$ transitions.

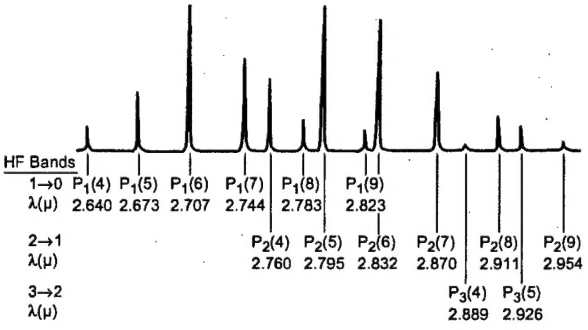

Figure 1. Spectral distribution of HF laser output (from Reference 1).

The rate coefficient for Reaction (1) is large, with a collision efficiency of ~10% at room temperature. This means that the rate of product formation is limited by the mixing of the separate flow streams containing reactant species. In addition, the excited states of HF(v,J) that are initially formed in the reaction are rapidly quenched by collisions with the surrounding species, including HF, the reactant species, and the carrier gases. This imposes requirements for rapid and efficient mixing of the reagent streams and high-speed, low-pressure flows to reduce the quenching in the optical resonator volume. Consequently, there is a need to optically diagnose the mixing field near the reagent injection point to characterize the effectiveness and stability of the system. The PSI hyperspectral imaging technique described in this paper provides direct views of the spatially distributed, state-to-state emission intensities and gains within the radiating volume, and

---

* Vice President, Applied Optics Enterprise, Member AIAA
† Principal Research Scientist, Member AIAA
‡ Principal Research Scientist
§ Principal Scientist

enables prompt evaluation of the chemical and optical performance.

We have implemented a hyperspectral infrared imaging instrument in quantitative observations of HF(v,J) emission in a laboratory chemical reactor and in the reaction zone and output beam of a supersonic chemical laser system.[2] This instrument, named AIRIS (Adaptive Infrared Imaging Spectroradiometer), consists of a low-order Fabry-Perot interferometer coupled to an infrared focal plane array and optical collection system. The device combines the imaging capability of an infrared camera with the spectral scanning capability of a rapidly scanned, medium-resolution Fabry-Perot etalon. The etalon is operated in low order, i.e., at mirror spacings on the order of the wavelength, so that the central spot of the transmitted Airy pattern fills the detector array with a spatially continuous image of the scene at each wavelength.[3] Rapid stepping of the etalon through a series of pre-programmed wavelengths produces a series of images of the scene at each wavelength, over a short (<1 second) time frame. These can be transformed into line-of-sight spectra of the emission intensity for each camera pixel's field of view. The high spectral resolution of the instrument, combined with a spectral fitting analysis, permits spectral isolation and quantification of the key transitions. Response-corrected infrared images at a succession of wavelengths are analyzed to generate maps of the spatial distributions of the radiating HF(v,J) states. This approach is further extended to produce spatial maps of population inversions and gains for specific transitions. In this paper, we describe methods for calibration and implementation of the measurements, and for processing and analysis of the hyperspectral data sets.

The laboratory measurements provide detailed characterization of an HF reactor under development at PSI. Rovibrationally excited HF(v,J) is generated by injection of H_2 into a co-flowing stream of F-atoms at 2.6 torr.[2] The F-atoms are produced by high-power, electrodeless, microwave discharge of SF_6 using a specially developed microwave source.[4] The interaction zone downstream of the H_2 injector generates intense HF(v,J) emission along a mixing length of some 9 cm, corresponding to a reaction time on the order of ~1 ms. High-resolution Fourier transform spectroscopy provides detailed diagnosis of the evolution of the excited state HF(v,J) population distributions as a function of distance downstream of the injector. Hyperspectral imaging measurements quantify the spatial distributions of the key laser transitions, and determine the regions of the flowfield with positive gain due to population inversions.

Instrument Description

A fully assembled AIRIS instrument is shown in Figure 2, illustrating the Fabry-Perot spectral filter, the optical collection system, and a liquid-nitrogen-cooled infrared camera. The operating principles of AIRIS are described in detail elsewhere,[2,3] and are illustrated in Figure 3. The AIRIS spectral filter consists of a high-finesse, low-order Fabry-Perot interferometer, and uses a pair of partially transmitting, high-reflectivity mirrors to generate interference patterns for a given mirror spacing. The mirrors used in this work are custom-coated for the 2.0 to 3.0 μm spectral region. (For other applications, additional mirror sets cover other wavelength ranges, e.g. 3.7 to 5.0 μm and 8 to 11 μm.) For collimated (or near-collimated) incoming light, the constructive and destructive interference patterns due to multiple reflections between the mirrors result in transmission of an Airy pattern of concentric rings, each containing a series of transmission fringes peaking at wavelengths which are integral multiples of the spacing between the mirrors. In the central spot, the integer order of each fringe is given (approximately) by twice the ratio of the spacing to the wavelength. The

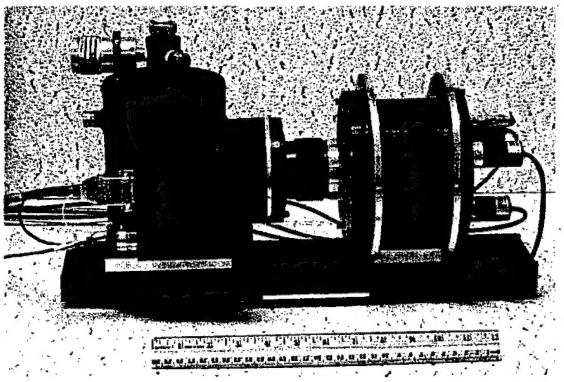

Figure 2. Photograph of an AIRIS instrument, consisting of Fabry-Perot filter, collection lens, and InSb camera/dewar system.

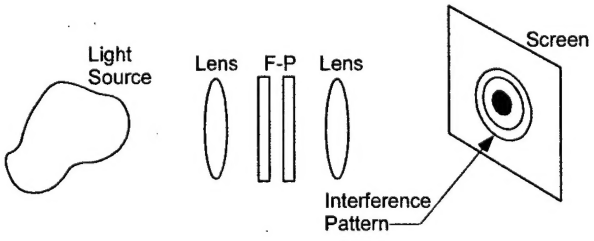

Figure 3. Typical arrangement for Fabry-Perot interferometers.

wavelength spacing between adjacent fringes is the free spectral range for the order corresponding to the longer of the two wavelengths, and defines a range of mirror spacings which can be used to scan spectrally within that order. The spectral resolution for each order is given by the ratio of the free spectral range to the etalon finesse; the finesse increases with mirror quality properties such as reflectivity, flatness, and parallelism.

When the etalon is operated in low order, where the mirror spacing approaches the wavelength, the Airy rings lie far off the optical axis, and the central spot fills the field of view of the camera detector array. This spot contains a spatially continuous image of the scene, viewed at peak wavelengths given by the mirror spacing and at spectral resolutions determined primarily by the mirror surface flatness and reflectance. In the infrared, this condition can be achieved using mirror spacings of a few μm, and with high angular acceptance compatible with focal plane IR detector array systems.

The AIRIS scanning mirror is driven at high precision (~4 nm) by a set of three piezoelectrically actuated inchworm motors. The mirror positioning and alignment are controlled by a computerized digital capacitance micrometry system which measures the mirror spacing and maintains parallelism. The mirror scanning and positioning system is calibrated for wavelength by observing the transmission fringes at high spectral resolution with a Fourier transform infrared (FTIR) spectrometer. For the hyperspectral imaging measurements described here, the AIRIS filter was operated in 10^{th} order, with a free spectral range of 0.26 μm and a spectral resolution of 0.01 μm.

The AIRIS optical system is illustrated schematically in Figure 4. A 50 mm zoom lens provides 1:24.5 magnification of the focal plane onto the object plane, which is some 60 cm in front of the lens. The infrared camera used in these measurements consists of a Cincinnati Electronics liquid-nitrogen-cooled InSb focal plane array, 120 pixels vertical by 160 pixels horizontal, each pixel 50 μm square. Given the magnification of the lens, the resulting field of view

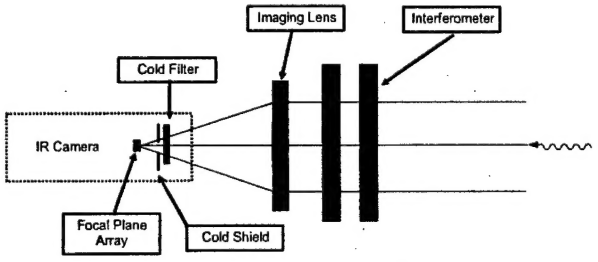

Figure 4. Schematic of AIRIS optical configuration.

is 14.7 cm vertical by 19.6 cm horizontal, with a single-pixel spatial resolution of 1.2 mm. A cold (77 K) interference filter, mounted inside the liquid nitrogen dewar, cuts off all radiation at wavelengths longer than 4.1 μm, thereby eliminating noise from room temperature background radiation. For order-sorting, an additional bandpass interference filter (not shown in the figure) is mounted in front of the entrance window of the interferometer, to limit the instrument bandpass to 2.65 to 2.9 μm, corresponding to one free spectral range in 10^{th} order. This permits observation of the $P_1(5\text{-}10)$, $P_2(1\text{-}7)$, and $P_3(1\text{-}4)$ lines, as well as a few of the lowest-lying $R_3(J'\text{-}1)$ transitions. Spectral images were obtained by stepping the etalon across its free spectral range at 0.01 μm increments, and recording an image after each step. The spectral responsivity of the instrument was calibrated for each pixel at each wavelength by recording full field images of a flat blackbody radiator of known temperature. This procedure generates a spectral responsivity data cube containing the ratio of the raw signal level to the blackbody radiance for each pixel at each wavelength.

Chemical Production of HF(v,J)

The rovibrationally excited HF(v,J) was produced in a low-pressure flow facility by injection of a H_2/He mixture into a co-flowing stream of F atoms. The F atoms were generated upstream of the injector by an electrodeless, 2.6 kW discharge of flowing SF_6/He mixtures in a high-power Microwave Driven Jet (MIDJet) device.[2,4] The source gas and diluent are fed into the discharge through a series of sonic injection nozzles. The design of these nozzles stabilizes the discharge along the axis of the MIDJet chamber and enables the device to operate over a large range of pressures and flow rates.

The H_2/He injector is mounted in the MIDJet chamber as shown in Figure 5. The injector is a 6 mm diameter stainless steel tube with four holes (0.5 mm diameter) spaced 1.5 cm apart. The injector assembly is water-cooled through an internal, coaxial 3 mm tube. Each of the four reagent injection orifices produces a supersonic flow of H_2/He from the exit plane to approximately 2 mm downstream. The axes of the injected reagent flows are aligned with the direction of the main flow from the discharge. The experiments were performed at 2.6 torr, with an SF_6 flow rate of 5.6 standard l/min and injectant flow rates of 0.54 and 12.0 standard l/min for H_2 and He, respectively.

As the injected H_2 stream expands and mixes with the surrounding flow of F atoms, Reaction (1) proceeds; prompt HF(v,J) emission appears within ~0.5 cm of the

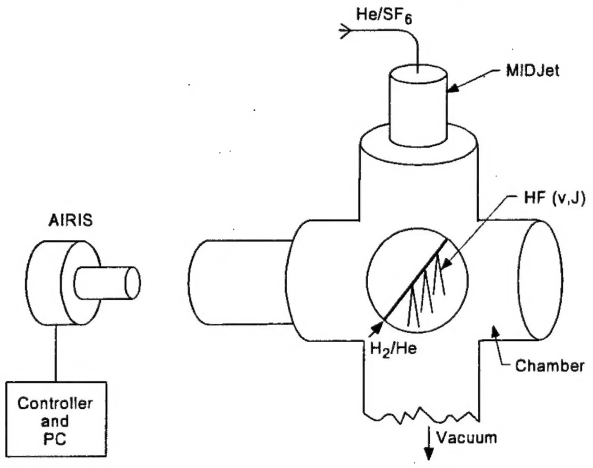

Figure 5. Block diagram illustrating MIDJet device and reagent injector.

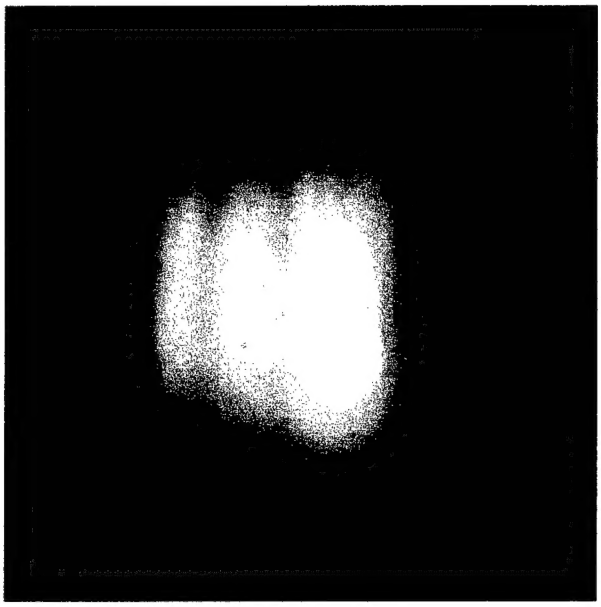

Figure 6. Processed image of emission from chemically produced HF(v=2, J=4), $P_2(5)$ transition, 2.795 μm. The image frame measures 14.7 cm vertical x 19.6 cm horizontal. Flow direction is from top to bottom of the image.

injection, and extends for some 9 cm downstream of the injection. The AIRIS instrument was positioned to view the chemiluminescent flame emission downstream of the injector through an infrared-transmitting window, as shown in Figure 5. The observed raw images were corrected for background radiation observed with the H_2/He flow turned off. This radiation was entirely due to thermal emission from apparatus hardware in the field of view; no molecular infrared emission within the spectral bandpass could be detected in the F-atom flow. The background-corrected images were further corrected for the instrument spectral response by dividing the background-subtracted raw signal levels by the spectral responsivity data determined in the black-body calibrations. The resulting processed images are expressed in absolute radiance units, W/(cm^2 sr μm), as a function of pixel horizontal and vertical coordinates, for each wavelength.

Spectral Images

A fully processed spectral image of HF emission from the $P_2(5)$ line (HF(v'=2, J'=4)), at 2.795 μm, is shown in Figure 6. The flow direction in the image is from top to bottom. The faint horizontal line above the flame is reflected light from the injector tube. The mixing of the F and H_2 flowfields is clearly evident, both in the individual injectant jets and in the merging of the product flow streams beginning ~1 cm downstream of the injector. The radiance observed at each point in this image is proportional to the product of the path-averaged number density of HF(2,4) in that location and the radiative emission rate for the transition. While horizontal transects of the image at different downstream locations give the progression of the mixing with flow distance, the vertical distributions in the intensity are governed by a balance of direct production of the HF(2,4) state by Reaction (1), cascade production by deactivation of higher states, and removal by collisional and radiative deactivation. The collisional deactivation processes will have an increasingly greater effect on the individual state populations as the flow distance and reaction time increase. Hence the emission intensity for HF(2,4) passes through a maximum at intermediate flow distance and decreases near the bottom of the image. A montage of spectral images across the spectral range of the measurements is shown in Figure 7. Spectral distributions extracted from three different flow distances are illustrated in Figure 8. The prominent features in the spectra are the $P_2(2\text{-}7)$ transitions. Less intense P_1 and P_3 transitions are also present but are not directly identifiable at this resolution (see below). The differences in the spectral distributions signify the deactivation of the initially produced HF(v,J) states as the reaction time progresses with flow distance. The actual reaction time at each point in the flame depends on the detailed mixing history upstream; however the linear flow velocity of the fully mixed gases indicates a maximum reaction time of ~1 ms at the bottom of the emitting region.

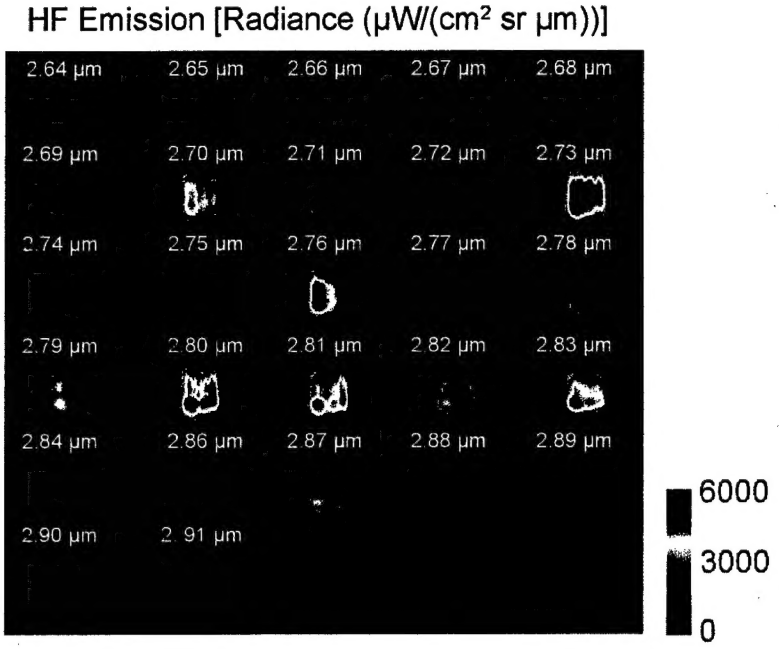

Figure 7. Montage of processed images of the HF(v,J) flame, scanning through a series of wavelengths. Flow direction is from top to bottom of each image.

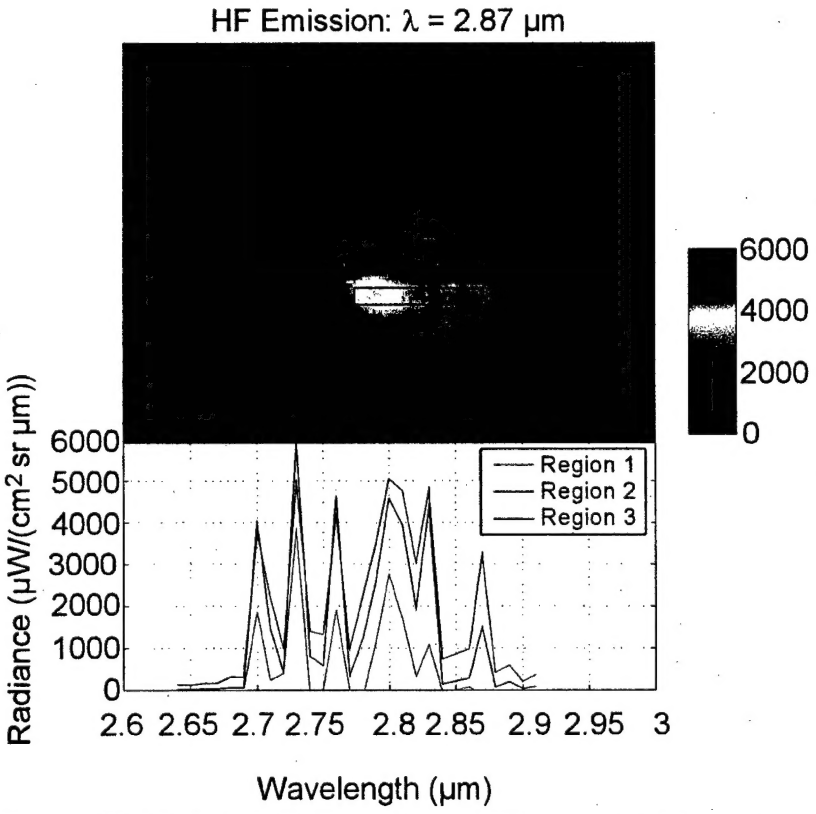

Figure 8. Processed image of HF(v'=2, J'=6), $P_2(7)$ emission at 2.870 μm, and AIRIS spectra corresponding to the horizontal regions indicated on the image. Flow direction is from top to bottom of the image. The sampled horizontal strips are 0.6 cm high and are located downstream of the injector at distances of 1.4, 4.5, and 6.3 cm for Region 1, Region 2, and Region 3, respectively.

Reaction (1) is known to produce HF(v,J) in state populations which are initially inverted, with most of the production occurring in v'= 2 and 3. As reaction time progresses, these initial populations cascade down into the lower states, resulting in increasingly relaxed state population distributions. Through examination of the spectral intensities of images like those in Figure 7, we can evaluate the extent of the state population inversions, and hence the small signal gain, throughout the reacting flowfield. For an optically thin system, the small signal gain for a given transition is proportional to the quantity (N' – fN"), where N' and N" are the upper and lower state number densities, and f is the ratio of the upper state and lower state degeneracies, in this case (2J'+1)/(2J"+1). For the $P_2(5)$ transition, the relative number density of the upper state, N', is given by the ratio of the observed radiance to the radiative rate for the transition. The lower state is HF(1,5), for which the relative number density N" can be obtained similarly, from the intensity of the $P_1(6)$ transition terminating in HF(0,6). We observe images of the $P_1(6)$ emission at 2.707 μm. Thus N' and N" can be determined for every point in the image of the HF(v,J) flame, and can be used to evaluate the small signal gain on the $P_2(5)$ transition. This is demonstrated in relative terms by the image in Figure 9. The relative statistically weighted population difference is positive over most of the flame image, and is largest between 1.5 and 5 cm downstream of the injector. The gain maximum is also located below the middle two jets, where contributions from the neighboring jets enhance the mixing of the reactants. Similar analyses can be performed for other cascade transition pairs, e.g., $P_2(6)$-$P_1(7)$ and $P_2(7)$-$P_1(8)$. Further analysis to determine small signal gains on an absolute basis is in progress.

Figure 9. Image of relative gain observed for the HF $P_2(5)$ transition. Flow direction is from top to bottom of the image.

FTIR Spectroscopy

We have also performed a detailed series of high-resolution spectroscopic measurements of the HF(v,J) emission in the MIDJet flame. These measurements employed a conventional Fourier transform infrared (FTIR) spectrometer, with a liquid-nitrogen-cooled InSb detector and a 3.5 μm short-pass filter to reduce radiometric noise from >300 K hardware in the field of view. The instrument was positioned similarly to the AIRIS instrument as shown in Figure 5, and viewed the HF flame with a collimated field of view ~5 cm in diameter. A horizontal slit aperture, 3 mm high and 6 cm long, was inserted into the chamber on a sliding probe, to permit masking of the field of view so that the flame could be viewed at specific distances downstream of the injector. This approach allowed us to obtain FTIR spectra of the horizontally averaged emission for different vertical distances downstream of the injector. In this way, we are able to observe the evolution of the HF(v,J) state population distributions as a function of flow distance. The spectral responsivity of the FTIR instrument was calibrated by obtaining spectra of a blackbody radiance source with the same viewing geometry as for the flame measurements. The FTIR instrument was operated at a spectral resolution of 0.5 cm^{-1}, which corresponds to approximately 0.00036 μm at 2.7 μm. The observed spectra were corrected for thermal background radiation and for spectral responsivity, to obtain absolute radiance units.

An FTIR spectrum of the emission from the flame, as viewed without use of the slit mask, is shown in Figure 10. The individual transitions for each vibrational level are labeled on the figure. As expected, R-branch and P-branch transitions from several rotational levels in each of the v = 1, 2, and 3 vibrational levels can be readily identified. The spectrum in this figure represents HF(v,J) emission viewed by the instrument from all points of the flame within the field of view. Example spectra obtained for two different flow distances using the slit mask are shown in Figure 11. The spectrum at short flow distance clearly shows a preponderance of emission from v' = 2 and 3, while the spectrum at the longer time shows substantial deactivation into v' = 1. As with the AIRIS images, preliminary analysis indicates significant population inversions and small signal gain on specific transitions. In particular, we infer positive gain throughout most of the observed reaction zone for the $P_2(4)$, $P_2(5)$, and $P_2(6)$ transitions. Further analysis of these spectra to determine detailed HF(v,J) state-by-state number densities and correlations to the AIRIS hyperspectral images is in progress.

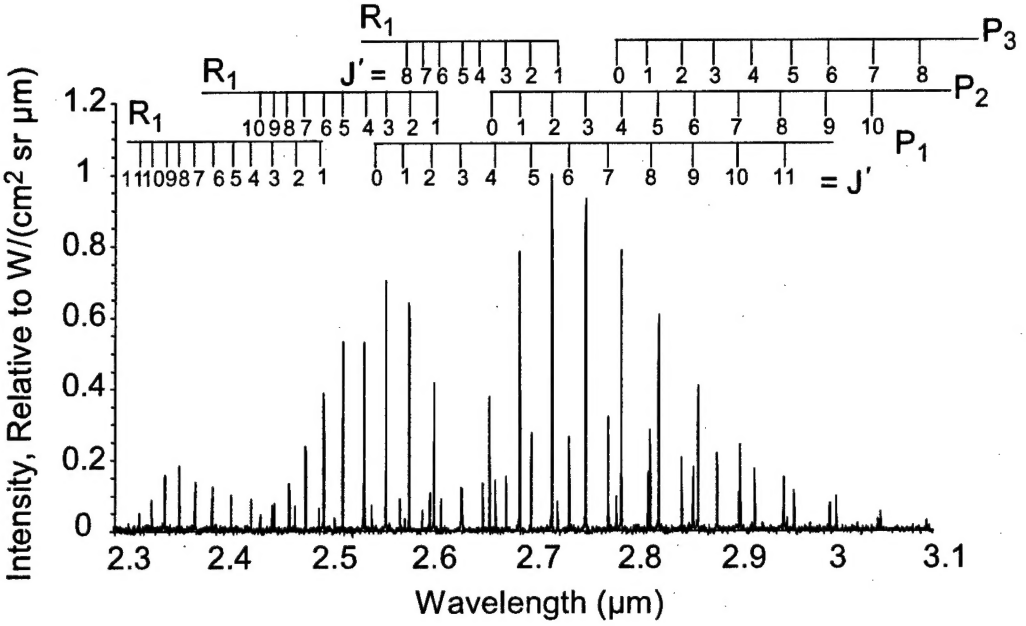

Figure 10. FTIR spectrum of HF(v,J) chemiluminescent emission from the F + H_2 interaction zone, averaged over the full field of view (no slit). Transitions are labeled according to upper-state vibrational and rotational quantum numbers, v' and J'. Intensities are proportional to radiance in W/(cm^2 sr μm), and are normalized to unity for the most intense feature.

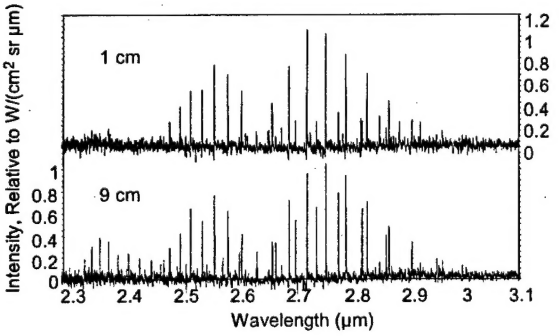

Figure 11. FTIR spectra of HF(v,J) chemiluminescent emission at two locations, 1 cm and 9 cm downstream of the injector. Intensities in each spectrum are proportional to radiance in W/(cm^2 sr μm), and are normalized to unity for the most intense feature.

Summary

We have described a novel diagnostic approach, utilizing hyperspectral infrared imaging, for probing chemically reacting flows to determine spatial maps of species concentrations, reagent mixing, and state population inversions. Using a subsonic flow reactor, we have obtained spatial and spectral distributions of chemiluminescent emission from rovibrationally excited HF(v,J) molecules formed in the reaction of H_2 with F. We have illustrated a method for processing these spectral images to obtain two-dimensional images of the population inversions and small signal gain relevant to specific HF laser transitions. This diagnostic method can also be applied to measurements of the spectral and spatial profiles of HF laser beams. We are continuing to develop an improved version of the hyperspectral imaging sensor described here, and plan to apply it to investigations of chemically generated HF(v,J) dynamics and HF laser characteristics.

Acknowledgements

We are grateful to the Air Force Research Laboratory Directed Energy Directorate, Kirtland AFB, NM, for support of this effort under Contracts F29601-01-C-0091 and F29601-02-C-0111.

References

1. Gross, R.W.F., and Bott, J.F., *Handbook of Chemical Lasers*, John Wiley and Sons, New York, 1976.

2. Rawlins, W.T., Oakes, D.B., Mulhall, P.A., Davis, S.J., Wright, R.F., Carroll, D.L., and Sentman, L.H., "Advanced Optical Diagnostics for HF Laser Development," Paper AIAA 2002-2221, AIAA 33rd Plasmadynamics and Lasers Conference, Maui, HI, May 2002.

3. Marinelli, W.J., Gittins, C.M., Gelb, A.H., and Green, B.D., "Tunable Fabry-Perot Etalon-Based Long-Wavelength Infrared Imaging Spectroradiometer," *Appl. Opt.* **38,** p. 2594, 1999.

4. Davis, S.J., Oakes, D.B., Read, M.J., and Gelb, A.H., "Atomic Fluorine Source for Chemical Lasers," *Gas and Chemical Lasers and Intense Beam Applications III*, S.J. Davis and M.C. Heaven, Editors, Proceedings of SPIE Vol. 4631 p. 178, January 2002.